Uniaxial incommensurate lattice of a quantum monolayer solid

J. M. Gottlieb and L. W. Bruch
Department of Physics, University of Wisconsin–Madison, Madison, Wisconsin 53706
(Received 10 March 1989)

Calculations are reported of the energy and structure of commensurate and uniaxially incommensurate monolayer lattices of molecular hydrogen and deuterium adsorbed on the basal-plane surface of graphite. The domain structure and energy for modulations driven by the periodic terms of the holding potential are determined. The calculations are based on a variational quantum-mechanical theory of a two-dimensional lattice and use the Silvera-Goldman model of the intermolecular potential. Results are in fair agreement with available experimental data.

I. INTRODUCTION

The monolayer solids of molecular hydrogen and deuterium physically adsorbed on the basal-plane surface of graphite are highly compressible quantum solids for which experimental data show[1–4] prominent effects of the competing periodicities of the adlayer and the substrate. An advantage of studying effects of mutual frustration of components of the interactions in the context of the adsorbed isotopic hydrogen series is that complex structures arise from relatively simple interactions among the constituents. We report here the results of calculations of the ground-state energy and structure for a two-dimensional (2D) model of the quantum monolayer solids, and comparisons with experimental data[1–9] for hydrogen and deuterium.

The phase diagrams of monolayer solids of molecular hydrogen and deuterium adsorbed on the basal-plane surface of graphite, H_2/graphite and D_2/graphite, include several registry and orientationally ordered phases. A combination of experimental techniques has been used to identify phase boundaries and to confirm proposed structures: specific-heat measurements,[8,9] neutron scattering,[2–7] and low-energy electron diffraction.[1,2] At low temperatures, H_2 and D_2 condense on graphite in the $(\sqrt{3}\times\sqrt{3})R30°$ commensurate lattice with 4.26 Å nearest-neighbor spacing of the molecules and with the axes of the triangular adlayer lattice oriented at 30° to the axes of the triangular Bravais lattice of the graphite surface. Under compression, uniaxially registered adlayer solids are formed[1–5] and then triangular incommensurate solids.[1,6] The H_2 and D_2 cases have different successions of orientations of the adlayer relative to the substrate.[1,8] The uniaxially registered adlayer has domain walls which on average form a parallel array; diffraction experiments[1–4] show modulation satellites which reflect departures from the average adatom spacing along the direction perpendicular to the remaining registry. The extent of the departures, expressed as a width of the domain wall, is available from quantitative analysis[2–4] of the intensities of neutron-diffraction peaks. Thus, there is much information available on the nominally simple isotopic hydrogen layers, in a low-temperature regime where ground-state energy calculations are relevant.

In previous calculations for hydrogen monolayers,[10] we used the Lennard-Jones potential parameters of de Boer for the molecular interactions in a Jastrow variational approximation for the triangular lattice as a function of density. As for helium, this procedure leads to a fair account of much thermodynamic data with a simple interaction model. However, in the exploratory calculations performed in formulating this project we found negative bulk moduli in the model for uniform triangular lattices of D_2/graphite at densities less than 1.12 times the commensurate density ($\rho_c = 0.0636/\text{Å}^2$). Since including the substrate periodic potential removes a scaling in the variational quantum mechanics which is a major computational advantage of the Lennard-Jones model, we now use the modern Silvera-Goldman (SG) multiparameter potential model[11] for the molecule-molecule interaction.

The periodic-potential amplitude V_g for the molecule-substrate interaction at the minimum of the holding potential is a poorly known input to the calculations. We used several values for V_g, starting with a value obtained[12] from a Lennard-Jones model for the holding potential derived[13] from molecular-beam scatterings. The values are in a range to give[14] zone-center frequency gaps for commensurate H_2/graphite and D_2/graphite which are close to the gaps determined by inelastic neutron scattering.[6,7]

The usual Jastrow variational trial function[15] for a quantum solid contains two parameters which, roughly, are a pair correlation length and a Gaussian width for vibrations about the lattice sites. For the modulated uniaxially registered monolayer solid, we introduce a third parameter: a "wall width" l which is the characteristic length of a sigmoid distribution of misfit over rows of the repeating domain unit. The limit of zero wall width, very sharp domain walls, has the misfit concentrated at one row. The search to determine the optimal values of the three variational parameters involves repetitious Monte Carlo calculations.[16]

A very different approach to the determination of the structure and energy of a striped phase is the path-integral Monte Carlo calculation for adsorbed helium performed by Abraham and Broughton.[17] Such a formulation does not have the constraints imposed by a variational trial function, but has large computational require-

ments from the outset. As we discuss in Sec. IV B, optimizing the variational parameters in a more general trial function would require calculating quite small energy increments.

The organization of this paper is as follows: Section II contains a description of the interaction model, with the additions to the Silvera-Goldman potential arising from the monolayer setting. Section III contains a description of the striped, domain-wall, monolayer lattice and the parametrization used in this paper. Results of the calculations and comparisons to experimental data are given in Sec. IV and some concluding remarks are given in Sec. V. Summaries of results for the classical one-dimensional discrete chain and of the methods used to process the computational data are contained in the Appendixes.

II. THE INTERACTION MODEL

A. The pair potential

The Lennard-Jones (12,6) potential model with de Boer's parameters has been used[10] in many previous calculations for condensed phases of molecular hydrogen and has computational advantages[16] arising from its simple functional form. However, as noted in Sec. IV A, it leads to predictions of mechanically unstable triangular lattices of D_2/graphite at densities near the commensurate density. Because these may be artifacts of the model which could lead to unphysically large adlayer modulations, we now use the more detailed Silvera-Goldman interaction model.[11] The Silvera-Goldman model is successful in accounting for a wide range of data for three-dimensional bulk phases[18] of hydrogen and deuterium; for 2D D_2 it has mechanically stable triangular lattices of nearest-neighbor spacings up to 4.22 Å. In this section we define the model and summarize what is known for it in the 3D dense phases.

The Silvera-Goldman interaction is a semiempirical isotropic effective pair potential for dense molecular hydrogen and deuterium. The potential energy of the many-body system is

$$\Phi_s(r_1,\ldots,r_N)=\sum_{i<j}\phi(r_{ij}) , \tag{2.1}$$

with

$$\phi(r)=\phi_{\text{pair}}(r)+(C_9/r^9)f_c(r) , \tag{2.2}$$

$$\phi_{\text{pair}}(r)=\exp(\alpha-\beta r-\gamma r^2) -(C_6/r^6+C_8/r^8+C_{10}/r^{10})f_c(r) , \tag{2.3}$$

$$f_c(r)=\exp[-(1.28r_m/r-1)^2], \quad r<1.28r_m$$
$$=1, \quad r>1.28r_m , \tag{2.4}$$

where $r_m=3.41$ Å is the separation of the minimum of ϕ_{pair}. The parameters in Eqs. (2.2)–(2.4), in atomic units, are $C_6=12.14$, $C_8=215.2$, $C_{10}=4813.9$, $\alpha=1.713$, $\beta=1.5671$, $\gamma=0.009\,93$, and $C_9=143.1$. They were determined from a combination of theoretical calculations and fits to experimental data. The separation at the minimum and at the zero of ϕ_{pair} are 3.41 Å and 2.97 Å, respectively, while the values for the Lennard-Jones potential[10] are 3.32 Å and 2.96 Å.

The first term in ϕ_{pair} represents a short-range overlap repulsion and the second term a van der Waals attraction. The cutoff function $f_c(r)$ serves to eliminate the divergence of the multipoles at the origin and to dampen the van der Waals attraction in the region of the pair-potential minimum, in accord with other modeling. It enables an interpolation through the potential minimum by a sum of terms based on large and small separation limits.

The constants[11] C_6, C_8, and C_{10} were calculated by Meyer. Silvera and Goldman determined the parameters α, β, and γ by fitting an experimental P-V isotherm of solid D_2 for pressures of 0–20 kbar and the zero-pressure sublimation energy of D_2, subject to a requirement that the small separation limit of the interaction agrees with self-consistent field calculations. The pair potential then reproduced differential cross-section data.

The C_9 term is an approximation to the many-body energies in the solid phases. It is a simplification of the Axilrod-Teller-Muto triple-dipole potential,[19] which scales as the cube of the 3D density. Silvera and Goldman introduced the approximation to facilitate their computations, although they noted that second-order quantities such as the speed of sound may be sensitive to this simplification. Their value $C_9=143$ a.u. reflects three-body lattice sums on the 3D lattice; in the monolayer calculations we use a value $C_9=29.7$ a.u. derived from the corresponding sums for the triangular lattice.

Since the construction of the SG model, there have been further constructions,[20,21] with an emphasis on high pressures, small molar volumes, and high temperatures, for phenomena such as high-pressure melting and shock-wave propagation. In the monolayer solids treated here, the nearest-neighbor separation is generally larger than 3.5 Å, which corresponds to a 3D solid of molar volume greater than 18 cm^3/mol and a 3D pressure of less than 2 kbar at low temperatures. Young *et al.* showed[20] that the SG model describes isotherms of solid H_2 and D_2 very well up to pressures of 20 kbar. Norman *et al.* compared[21] the SG model with later models and concluded that it treats large molar-volume data with an accuracy comparable to that of the later models.

Thus, there is an extensive documentation[11,18,20,21] for the SG model in 3D dense phases showing it to be a rather accurate approximation to the isotropic pair interaction of isotopes of molecular hydrogen. Novaco[14] used it in his calculations of the dynamics of the commensurate monolayer and we concluded that it had sufficient validity to warrant the extensive calculations needed to determine the structure of the uniaxially incommensurate monolayer. The energy and length scales of the SG model are set by fitting to the 3D solid; for the modulated monolayer, these scales are balanced against those in the holding potential.

B. Holding potential and substrate effects

The ground-state energy for a single H_2 or D_2 adsorbed on graphite is derived from measurements[13] of selective

adsorption resonances. For H_2/graphite it is -482 K and for D_2/graphite it is -516 K. The experimental data do not directly yield the leading Fourier amplitude V_g of the lateral variation of the holding potential at the equilibrium height; a value $V_g=-6.4$ K was estimated[12] from a model for the holding potential, with an average over zero-point motion in the perpendicular direction. Because such modeling underestimates the corrugation for other adsorbates on graphite, we have performed the calculations for several values of V_g in the range -6.4 to -9.6 K.

The periodic potential experienced by one molecule is expressed in terms of V_g by

$$U_{\rm per}(\mathbf{r})=V_g\sum\exp(i\mathbf{g}\cdot\mathbf{r})\ , \tag{2.5}$$

where $\mathbf{r}$ is the lateral (2D) position, measured relative to a commensurate lattice site, and the sum runs over the first shell of six reciprocal lattice vectors of the substrate, of magnitude g_0 ($=2.95$ Å^{-1} for graphite).

The corrugation amplitude V_g is poorly enough known that we do not attempt to model its dependence on the distance from the substrate. Correspondingly, the monolayer is modeled as a two-dimensional planar solid, with no allowance for a possible "warping" of the monolayer by displacements perpendicular to the substrate in the domain-wall regions where the smallest nearest-neighbor spacings occur. However, except for the largest values of V_g, the smallest spacings in these calculations are larger than the monolayer limit of compression[6,10] of the triangular lattices.

The van der Waals attraction between adsorbed molecules is reduced from its value in the 3D gas by the electrodynamic screening response of the substrate, the McLachlan interaction.[19] We estimate its effect by calculating also for an effective value of $C_6=9.94$ a.u., rather than 12.14 a.u., in $\phi_{\rm pair}$ to mimic the contribution of the McLachlan interaction at lateral spacings of 3.4–4.3 Å and an overlayer height relative to the image plane of 1.5 Å. With this modification the minimum and zero of $\phi_{\rm pair}$ occur at 3.50 Å and 3.06 Å, respectively.

III. QUANTUM-SOLID THEORY

A. Adlayer structures

Most previous work for quantum monolayer solids has been limited to treating adlayers on structureless substrates or to the specific case of the commensurate $(\sqrt{3}\times\sqrt{3})R30°$ lattice. Such triangular lattices are included in the present work.

We now describe a specific nontriangular adlayer lattice modulated by the periodic potential of the substrate, the so-called striped structure of the uniaxially incommensurate adlayer. It arises from the competing periodicities of two lattices, the intrinsic triangular lattice of the adlayer and the surface lattice of the substrate—here a triangular Bravais lattice for the basal-plane surface of graphite. We summarize the geometric definition of the stripes, the identification of the associated energy, and the diffraction signature of the structure.

The statistical mechanics of striped lattices and of disordered domain-wall arrays has been treated by Halpin-Healy and Kardar,[22] with reference to the phase diagram of helium adsorbed on graphite. In their lattice-gas model, a domain-wall fluid phase is intermediate to the commensurate and uniaxially incommensurate lattices. In the present zero-temperature modeling, we neglect the domain-wall fluid. A consequence of this omission and of omitting vacancy effects may be that the calculated step in the chemical potential from the value at condensation in the commensurate lattice to the threshold for finite misfit would be rounded at finite temperatures.

The striped domain structure arises under uniaxial compression of the $(\sqrt{3}\times\sqrt{3})R30°$ commensurate adlayer along the substrate y axis shown in Fig. 1. In terms of the x and y axes of Fig. 1, the primitive reciprocal lattice vectors of the triangular surface lattice are

$$\mathbf{g}_1=g_0\hat{\mathbf{x}} \tag{3.1}$$

and $\mathbf{g}_2=g_0[\frac{1}{2}\hat{\mathbf{x}}+(\sqrt{3}/2)\hat{\mathbf{y}}]$, with $g_0=4\pi/L\sqrt{3}=2.95$ Å^{-1} for $L=2.46$ Å, the side of the graphite surface unit

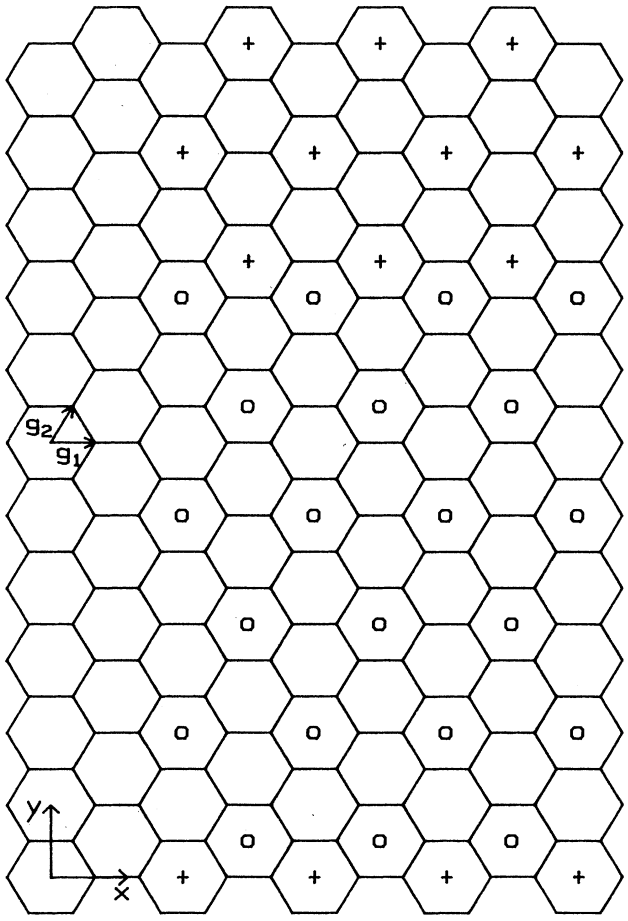

FIG. 1. Schematic diagram illustrating the orientation of a six-row uniaxially compressed monolayer with superheavy domain walls relative to the surface honeycomb lattice of the basal-plane graphite. The primitive reciprocal-lattice vectors of the graphite surface and the x and y axes of the coordinate system used in Sec. III are shown.

cell. The average positions in the adlayer lattice have x components

$$R_x(\alpha)=nL_c$$

and (3.2)

$$R_x(\beta)=(n+\tfrac{1}{2})L_c$$

in alternating rows α and β, and y components

$$R_y=m(\sqrt{3}/2)L_c+v(m)\ , \tag{3.3}$$

where n and m are integers, $L_c=4.26$ Å.

The increment $v(m)$ is zero in the commensurate lattice. For the uniform uniaxially incommensurate lattice, $v(m)$ is a linear function of the row index "m," while in the striped structure $v(m)$ is a succession of sigmoids as a function of m. For a structure consisting of domains of $2\bar{n}$ rows separated by parallel superheavy domain walls, as proposed[1-4] for H_2/graphite and D_2/graphite, the function $v(m)$ has a periodicity

$$v(m+2\bar{n})=v(m)-\tfrac{2}{3}(\sqrt{3}/2)L_c=v(m)-L\ , \tag{3.4}$$

and the fractional mean misfit of the average spacing of the rows relative to the commensurate row spacing of $(\sqrt{3}/2)L_c$ is

$$\overline{m}=-1/(3\bar{n})\ . \tag{3.5}$$

The average density relative to the commensurate density is

$$\rho/\rho_c=1/(1+\overline{m})\ . \tag{3.6}$$

A periodically repeated patch of N_y rows then has $N_y/(2\bar{n})$ walls. The total length of walls is, with N_x atoms in each row and total number N atoms in the patch,

$$N_xL_cN_y/(2\bar{n})=NL_c/(2\bar{n})\ . \tag{3.7}$$

The energy per unit length of the walls is derived from the difference between the energy of the striped lattice and the energy of the commensurate lattice, both calculated for the same number N of particles:

$$w=\{[E(\text{stripe})-E_c]/N\}(2\bar{n}/L_c)\ . \tag{3.8}$$

This construction gives the intrinsic energy per unit length of well-separated walls in the limit of large $\bar{n}$, but at finite $\bar{n}$ the energy difference includes interaction energy between the walls. We use $\bar{n}=3$, domains of six rows, in the calculations and argue in Sec. IV B that the walls are narrow enough, and the wall-wall interactions are small enough, that Eq. (3.8) gives a good approximation to the intrinsic wall energy.

To the extent that Eq. (3.8) leads to an energy w which is approximately independent of $\bar{n}$ for large $\bar{n}$, the energy E(stripe) varies linearly with small mean misfit

$$E(\text{stripe})\simeq E_c-\tfrac{3}{2}NL_cw\overline{m}\ . \tag{3.9}$$

The energy increment for a uniaxially compressed lattice is thus expressed in terms of the energy and density of added walls.

We use Eq. (3.9), for low temperatures, to find the increment in chemical potential necessary to drive the adlayer incommensurate in a continuous transition. The adlayer first condenses in the commensurate lattice at a chemical potential given in terms of the calculated E_c by

$$\mu_c=E_c/N\ . \tag{3.10}$$

The zero-temperature grand potential for a system of N particles in a fixed area A and chemical potential μ is

$$\Omega=E-N\mu\ , \tag{3.11}$$

with coverage in terms of the number N_c in the commensurate layer

$$N=N_c/(1+\overline{m})\ . \tag{3.12}$$

Combining Eqs. (3.9)–(3.12) gives

$$\Omega\simeq N(\mu_c-\tfrac{3}{2}L_cw\overline{m}-\mu)\ ; \tag{3.13}$$

not until μ reaches a threshold

$$\mu_t=\mu_c+\tfrac{3}{2}L_cw \tag{3.14}$$

does an increase in the chemical potential cause a lowering of the grand potential by an increase of coverage. Such a step in the chemical potential may have been observed[23] for the onset of the striped phase of Xe/Pt(111).

The specification of the average row positions is contained in the function $v(m)$. An explicit expression[24] for $v(m)$ in the case of an isolated domain wall treated in continuum elasticity approximation is given in Eq. (A8). We use the following approximation to the function for a repeat unit of six rows with the domain wall centered between the third and fourth rows:

$$v(j)=-(L/2)\{1-\tanh[(3.5-j)/l_t]\}\ , \quad j=1,\ldots,6\ . \tag{3.15}$$

The smallest nearest-neighbor spacing occurs between atoms in the third and fourth rows and is

$$L_{\mathrm{NN}}=(L_c/2)(1+3\{1-\tfrac{2}{3}\tanh[1/(2l_t)]^2\})^{0.5}\ . \tag{3.16}$$

The parameter l_t is a variational parameter set by finding the minimum-energy structure; it measures the wall width in units of the commensurate row spacing 3.689 Å. The relation of Eq. (3.15) to the continuum solution[24] and to a solution[25] for a classical discrete lattice is discussed in Appendix A and in Sec. IV B.

The striped structure of parallel domains has a characteristic diffraction pattern which distinguishes it from the uniform uniaxially compressed lattice. The pattern may be described in terms of diffraction peaks associated with the superlattice of domains or, as here, in terms of the reciprocal-lattice vectors of the substrate and of the average adlayer lattice and the misfit wave vectors between the two families of reciprocal-lattice vectors. Primitive reciprocal-lattice vectors for the uniform uniaxial incommensurate lattice of misfit $\overline{m}$ are

$$\mathbf{t}_1=(g_0/2)\{\hat{\mathbf{x}}+\hat{\mathbf{y}}(1/[\sqrt{3}(1+\overline{m})])\}$$

and (3.17)

$$\mathbf{t}_2=(g_0/2)\{-\hat{\mathbf{x}}+\hat{\mathbf{y}}(1/[\sqrt{3}(1+\overline{m})])\}\ .$$

The $\mathbf{g}_1$ reciprocal-lattice vector of the substrate, Eq. (3.1), is thus in the lattice spanned by $\mathbf{t}_1$ and $\mathbf{t}_2$:

$$\mathbf{g}_1=\mathbf{t}_1-\mathbf{t}_2 , \tag{3.18}$$

and the misfit wave vector $\mathbf{q}$ is defined relative to the vector $\mathbf{g}_2$ by

$$\mathbf{q}=(2\mathbf{t}_1+\mathbf{t}_2)-\mathbf{g}_2=(2\pi/L)[-\bar{m}/(1+\bar{m})]\hat{\mathbf{y}} . \tag{3.19}$$

The relative diffraction intensities from the layer for wave vectors $\mathbf{t}_3=\mathbf{t}_1+\mathbf{t}_2$, $\mathbf{t}_3+\mathbf{q}$, $\mathbf{t}_3-\mathbf{q}$, $\mathbf{t}_1$, $\mathbf{t}_1+\mathbf{q}$, and $\mathbf{t}_1-\mathbf{q}$, calculated from the static structure factor

$$S(\mathbf{k})=\left\langle \left| \sum_j \exp(i\mathbf{k}\cdot\mathbf{r}_j) \right|^2 \right\rangle \Big/ N^2 , \tag{3.20}$$

are reported in Table III and Sec. IV B. In Eq. (3.20) the expectation value is performed for the optimized ground-state trial function and the sum extends over the N particles in the Monte Carlo cell. The relative intensities in neutron-diffraction experiments have been used[2-4] to estimate the wall-width parameter for D_2/graphite and H_2/graphite; comparisons with the data are given in Sec. IV B.

The frequency gap for lateral (2D) vibrations at the center of the Brillouin zone for the commensurate adlayer can be estimated[26] with an adiabatic approximation in which the force constant is calculated for small displacements of the adlayer center of mass. If relaxation of the ground-state wave function during the displacement is neglected, the result is formally the same as the expression for the zone-center frequency used in Novaco's self-consistent phonon theory[14] of the adlayer. The angular frequency of molecules of mass M is

$$\Omega=g_0[-3V_g\langle \exp(i\mathbf{g}_0\cdot\mathbf{r})\rangle/M]^{0.5} , \tag{3.21}$$

with the ground-state expectation value for one of the primitive reciprocal-lattice vectors of Eq. (3.1) and displacements $\mathbf{r}$ from a commensurate lattice site. In this approximation, the zone-center frequency is simply related to the contribution of the surface corrugation to the ground-state energy of the commensurate lattice.

B. Variational trial function

The basic calculation is to determine the ground-state energy for a structure of specified average density. We use a variational approximation[15] and a generalization of the Jastrow trial function for a uniform lattice.[10] The trial many-body wave function has the form

$$\Psi=\exp\left[-\tfrac{1}{2}\sum_{i<j}(b/r_{ij})^5-(A/2)\sum_j v_j^2\right] , \tag{3.22}$$

where the r_{ij} are the interparticle distances in each configuration and the $\mathbf{v}_j=\mathbf{r}_j-\mathbf{R}_j$ are the displacements from the average lattice positions $\mathbf{R}_j$. The variational parameters are the constants b and A and the wall-width parameter l_t, Eq. (3.15), which sets the displacements of the average row positions from the positions in the uniform, nonmodulated lattice. In this trial function the parameters A and b are the same for all rows.

The expectation value of the Hamiltonian is calculated by now-standard Monte Carlo methods.[15,16] The Hamiltonian is separated into the kinetic-energy operator, the repulsive and attractive functional terms of the pair potential Eq. (2.3), the pair approximation to the three-body energy, and the periodic substrate potential. The expectation values are separately calculated and smoothed with the procedure described in Appendix B. Sums of two-body terms, the pair potential and the Jastrow kinetic-energy term, are performed for the particles in the basic Monte Carlo cell, with a nearest-image rule; no continuum end correction is made for the contribution of more distant pairs.

IV. RESULTS

A. Triangular adlayer lattices

The variational ground-state energies for the commensurate $(\sqrt{3}\times\sqrt{3})R30°$ lattice, E_c, and for the intrinsic triangular lattice on a smooth substrate, E_0, give a first test whether the commensurate lattice is the ground state of the model and also a measure of the contribution of the corrugation energy V_g. The results, listed in Table I, show that in all the cases the commensurate lattice has lower energy than the intrinsic lattice. Zero-point oscillations of the molecules about the lattice sites greatly reduce the average corrugation energy: For $V_g=-6.4$ K, the minimum of the periodic potential energy is -38 K, while the expectation value of the periodic potential energy for H_2 is -15 K and for D_2 is -19 K.

Interpolating in the results for $D_2(a)$, the "bare" interaction model, gives an estimate of -3.4 K for the corrugation amplitude at which the commensurate lattice has lower energy than the intrinsic unmodulated lattice; the critical magnitudes for the other cases are smaller. Such comparisons provide lower bounds on the critical magnitude of V_g for stability of the commensurate lattice; stability relative to the modulated lattice is tested by the sign of the wall energy per unit length, Sec. IV B.

A necessary condition for mechanical stability of a lattice is that the bulk modulus be positive. The bulk modulus calculated for uniform triangular lattices of D_2 with the de Boer–Lennard-Jones potential[10] is negative for lattice constants larger than 4.02 Å, i.e., at densities within 12% of the commensurate density. To the extent that this feature is an artifact of the Lennard-Jones model, there would be concerns about related artifacts in calculations for the striped configuration with average density $1.125\rho_c$. As a preliminary study of the SG model, we calculate the bulk modulus of uniform triangular lattices of H_2 and of D_2, on a structureless substrate. The bulk modulus is positive for densities down to ρ_c in three of the four cases of Table I; for $D_2(a)$, it becomes negative at $1.02\rho_c$. The results are shown in Table I for three densities: The deuterium is more compressible than the hydrogen at each density; domain walls for average densities in this range are expected to be sharper for D_2 than for H_2.

The frequencies for the zone-center gap of the commensurate layer, calculated with Eq. (3.21), are listed in Table I. The values found by Novaco[14] in a self-

TABLE I. Triangular lattices of hydrogen and deuterium, Silvera-Goldman potential model.[a]

V_g[b]	Property	$H_2(a)$	$H_2(b)$	$D_2(a)$	$D_2(b)$
0	E_0[c]	−25.1	−12.5	−45.4	−28.1
	L_0[c]	4.09	4.32	3.78	3.98
0	E_c[d]	−24.3	−12.4	−37.4	−26.1
$1V_g(0)$	E_c	−35.6	−24.6	−52.5	−42.1
	ω[e]	39.1	39.8	31.2	31.6
$1.4V_g(0)$	E_c	−41.8	−30.9	−60.2	−50.0
	ω	48.5	49.2	38.5	39.6
0	B[f](ρ_c)	14.4	22.1	−1.8	4.7
	$B(1.09\rho_c)$	26.6	37.0	9.0	19.4
	$B(1.22\rho_c)$	54.8	70.8	39.2	59.0

[a]Silvera-Goldman model as defined in Sec. II. Case (a): $C_6=12.14$ a.u.; case (b): $C_6=9.94$ a.u.
[b]Corrugation amplitude for Eq. (2.5); $V_g(0)=-6.4$ K (Ref. 12).
[c]Energy (in K) per particle and nearest-neighbor spacing in Å, of the minimum-energy intrinsic triangular lattice.
[d]Energy (in K) per particle of the $\sqrt{3}$ commensurate lattice.
[e]Brillouin zone-center frequency gap (in K) for lateral motion, calculated with Eq. (3.21).
[f]Bulk modulus in erg/cm^2 of uniform triangular lattices with density stated as a multiple of the commensurate density $\rho_c=0.0636/\text{Å}^2$.

consistent phonon approximation for a model similar to our case (a) are 36.9 K for D_2 and 46.6 K for H_2. Novaco reexamined the averaging to set the value of V_g and used somewhat different values (-7.7 K for H_2 and -8.1 K for D_2) than the reference value[12] -6.4 K here; interpolation in the values of Table I shows satisfactory agreement with his results. The gap values from neutron scattering measurements are 47 K (Ref. 6) and 41 K (Ref. 7) for D_2 and 57 K (Ref. 6) for H_2; thus the 2D corrugation amplitude V_g needed to reproduce the data is slightly larger than the largest value (-9.6 K) used in our calculations.

The mean-square lateral displacement for commensurate D_2/graphite is reported[7] to be 0.25 Å^2. The model calculations for case (a) give 0.65 and 0.59 Å^2 for $V_g(0)$ and $1.4V_g(0)$, respectively [and 0.63 and 0.57 Å^2 in case (b)]. A comparison by Frank *et al.*[7] to the mean-square displacement for Hartree calculations[10] is misleading: The optimized Jastrow trial function gives values which should supersede the results of the Hartree approximation.

The chemical potential at monolayer condensation into the commensurate lattice is constructed as the sum of the ground-state energy of the lateral structure, E_c in Table I, and the ground-state energy for a single molecule in the holding potential,[13] -482 K for H_2/graphite and -516 K for D_2/graphite. The result for H_2/graphite is $\mu_c\sim-520$ K, a value in good agreement with estimates of -510 to -540 K obtained by Motteler[9] from extrapolation of vapor pressure data. For D_2/graphite the result is $\mu_c\sim-570$ K.

We have not repeated the calculations[10] of the monolayer limit of compression. An estimate based on comparing the length scale in ϕ_{pair} with that in the Lennard-Jones model is that the smallest nearest-neighbor spacings of the triangular monolayer lattice for the Silvera-Goldman model are 0.05–0.1 Å larger than those[10] for the Lennard-Jones model.

B. Uniaxially incommensurate lattice

Specific-heat data[8] for both H_2/graphite and D_2/graphite show the existence of an α phase at low temperatures for densities in the range $(1\text{–}1.2)\rho_c$. Diffraction data[1–4] show the α phase is a uniaxially incommensurate lattice.

We calculate the ground-state energy for the uniaxially incommensurate lattice shown schematically in Fig. 1: a lattice of average density $1.125\rho_c$, with mean linear misfit $-\frac{1}{9}$ and domains of six rows of molecules. The Monte Carlo calculation has periodically repeated cells of 144 particles, arranged in 12 rows of 12 particles and in two domains ($\tilde{n}=3$). The variational calculation has one parameter, l_t, to set the displacements of rows in the domains; presumably the energy minimization is most sensitive to the smallest nearest-neighbor spacings.

The energy per unit length w of the walls obtained, using Eq. (3.8), from the calculated ground-state energy and the ground-state energy of the commensurate lattice is shown in Fig. 2 as a function of the corrugation amplitude. The values of w are positive, which establishes the stability of the commensurate lattice against spontaneous formation of such walls. Under linear extrapolation of the data shown in Fig. 2, the wall energy vanishes at a threshold corrugation amplitude of -3.9 K for $D_2(a)$ and -0.3 K for $D_2(b)$. Such magnitudes are much smaller than modeling[13,12] of the holding potential indicates and than the magnitudes needed[14] to fit the measured zone-center frequency gap, so that the commensurate lattice is assured as the minimum-energy structure for this interaction model.

The values of the wall-width parameter l_t in Table II correspond to sharp domain boundaries: For most of the cases 40% or more of the misfit is concentrated between the most closely spaced rows [rows 3 and 4 in Eq. (3.15)]. The interaction energy between walls separated by six rows in Joos's solution[25] for the 1D Frenkel-Kontorova

chain, adjusted to the same scaled nearest-neighbor spacing as for the entries in Table II, is less than 5% of the single-wall energy. To estimate the effect of the 2D extent of the walls we integrate over line segments with the exponential variation fitted by Joos:[25] The wall-wall energy for the six-row domain may be as much as 10% of the wall energy for the D_2 cases and up to 20% for the H_2 cases. The wall-wall energy is included in the energy w calculated with Eq. (3.8), and therefore the chemical potential step calculated with Eq. (3.14) is larger than the value which would be obtained if the wall interaction energy had been isolated. Also, the Peierls pinning potential for the domain walls appears to be very small in these cases: With Joos's solutions,[25] chosen in the same way as for estimating the wall interaction energies, the pinning potential energy is less than 2% of the wall energy.

An important simplification in the trial function, Eq. (3.22), is that the Gaussian width A and the correlation scale b are the same for all rows. To explore how serious this constraint is, we note that the optimized A and b differ from their values in the commensurate lattice by 8 and 3.5 %, respectively, for the H_2 cases and by 8 and 7.5 %, respectively, for the D_2 cases. As a scale, 1% changes in the trial energy for the domain structure arise under changes of A by 15% (H_2) and 25% (D_2) and of b by 3% (H_2) and 5% (D_2). We infer that to optimize the variational parameters in an elaboration of the trial function with different values of A for different rows in the domain would require tracking quite small variations in the Monte Carlo expectation values. If such a detailed picture of the domain is needed, it appears that another technique such as the quantum path-integral method of Abraham and Broughton[17] should be used.

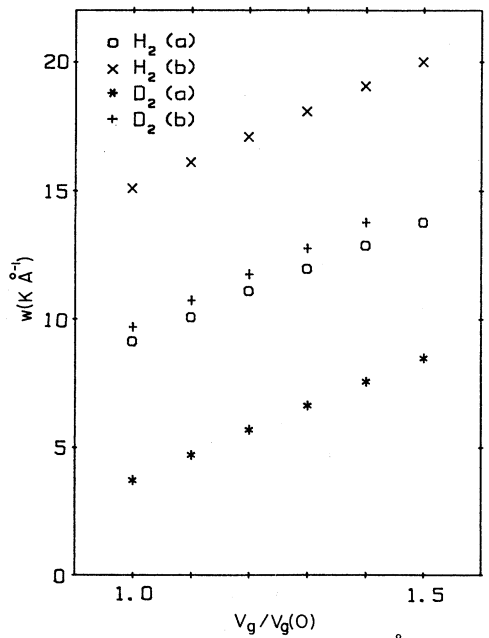

FIG. 2. Wall energy per unit length, in K/Å, of the modulated uniaxial incommensurate lattice as a function of the corrugation amplitude, scaled by $V_g(0) = -6.4$ K, Ref. 12. Energies derived from the calculations using Eq. (3.8) are shown for H_2 and D_2 for two interaction models: Case (a) is the Silvera-Goldman model as defined in Sec. II A, and case (b) is the modified model with $C_6 = 9.94$ a.u., to include adsorption-induced modifications of the van der Waals attraction.

TABLE II. Parameters of the domain-wall structures.[a]

	$H_2(a)$	$H_2(b)$	$D_2(a)$	$D_2(b)$
$1V_g(0)$[b]				
w[c]	9.1	15.1	3.7	9.7
$\Delta\mu_t$[d]	58.4	96.4	23.8	62
l[e]	1.40	1.46	1.07	1.14
L_{NN}[f]	3.56	3.58	3.38	3.42
$1.4V_g(0)$[b]				
w[c]	12.9	19.1	7.6	13.8
$\Delta\mu_t$[d]	82.2	122	48.3	88
l[e]	1.17	1.23	0.93	0.99
L_{NN}[f]	3.44	3.47	3.27	3.32

[a]SG interaction model, with cases as in Table I; for six-row domain of mean misfit $-\frac{1}{9}$.
[b]Corrugation amplitude in units of -6.4 K.
[c]Wall energy per unit length, in K/Å, calculated for six-row domain with Eq. (3.8).
[d]Step in chemical potential, from value at condensation, to drive nonzero misfit, Eq. (3.14).
[e]Wall-width parameter, in units of 3.689 Å, for Eq. (3.15).
[f]Nearest-neighbor spacing, in Å, between molecules in the most closely spaced rows in the domain.

The energy per unit length of the walls, the wall-width parameter, the smallest mean nearest-neighbor separation in the domain, and the step in the chemical potential to create finite misfit [Eq. (3.14)] are listed in Table II for several cases. The nearest-neighbor spacings for the larger corrugation cases in Table II are less than the values[6] for triangular lattices at the monolayer limit of compression, 3.51 Å (H_2) and 3.40 Å (D_2), which may indicate a need to include the three-dimensional character of the monolayer in such cases.

The chemical potential at monolayer condensation[9] of H_2/graphite is about -520 K and the bulk chemical potential is[18] -133 K for D_2 and -90 K for H_2. For H_2/graphite, Motteler[9] found by an analysis of vapor-pressure and specific-heat data that the chemical potential increases to -390 K at density $1.2\rho_c$ and to -280 K at $1.4\rho_c$. There was no indication of a sharp step in the chemical potential, Eq. (3.14), in his analysis, but his primary vapor-pressure data were for temperatures above 15 K and the α phase occurs[8] only below 10 K so that thermal effects may be important for the comparison. We have calculated the chemical potential for the intrinsic triangular lattices of H_2 discussed in Sec. IV A, without including effects of the substrate periodicity. For an area of 13 Å^2/mol ($1.2\rho_c$), the increase of chemical potential from μ_c is 50 K [case (a)] and 100 K [case (b)]; comparing to $\Delta\mu_t$, Table II, indicates the α phase may be unusually compressible.

The calculated increment in chemical potential to drive the commensurate lattice to nonzero misfit is small enough that there should be, as observed,[9] a large chemical potential range available to the incommensurate monolayer before further condensations occur.

The domain-wall width has been derived by fitting[2–4]

the relative intensities of diffraction peaks for neutron scattering from monolayers of average density close to the $1.125\rho_c$ case. The values reported[2-4] for the parameter l_F in the continuum approximation to the row displacements, Eq. (A8), are 10.3 Å ($l_F=0.888$) for H_2 and 9.2 Å ($l_F=0.792$) for D_2. The corresponding smallest nearest-neighbor spacings are 3.56 Å (H_2) and 3.49 Å (D_2). The variational parameters l_t which give rise to these spacings, $l_t=1.41$ (H_2) and $l_t=1.26$ (D_2), are not far from the values listed in Table II. As a measure of the sensitivity of the variational calculation to the choice of l_t, we note that the trial energy varies by only 1% under 20% changes in l_t.

Results of calculations of the structure factor for several wave vectors related to the reciprocal lattice vector of the average lattice and to the misfit wave vector, Eq. (3.19), are presented in Table III for the case $V_g=-6.4$ K, in the form of the normalized structure factor (equal to 1 at the reciprocal-lattice vectors of a static uniform lattice). There are also entries related to ratios of the quantum expectation values to the classical values for a static lattice with the same average positions,

$$R_{\rm SF}=-(1/k^2)\ln[S(k)/S(k,\text{static})] \ . \tag{4.1}$$

$R_{\rm SF}$ for a peak at wave vector $\mathbf{k}$ is closely related to the Debye-Waller factor; in the absence of multiphonon processes it would be constant.

With Eq. (3.15) for the row displacements, the ratio of the intensity of peak 4 to peak 3 increases and that of peak 6 to peak 3 decreases as l_t increases. Similar trends are found in static lattice calculations with two other functional forms for the distribution of misfit among rows in the domain: If the parameters l_F and l_J, in Eqs. (A8) and (A13), respectively, are adjusted to make the solutions have the same smallest nearest-neighbor spacing as for Eq. (3.15), the ratio of intensity of peak 4 to peak 3 is the same, to 10%, for the three functions. For the less intense peaks listed in Table III, there are differences up to about 30% for the relative intensities from the three functions. The differences for the functions from Eqs. (A8) and (A13) range up to about 20%. For future data analyses, a method which includes the discreteness of the lattice in the functional distribution of misfit in the domain and involves only modest calculations might be to use the solution of Eq. (A13) and adjust l_J to fit the experimental relative intensities.

The neutron-diffraction intensities from the D_2/graphite striped lattice are reported[2] as the ratio of the sum of the intensities of peaks 1 and 2 (as identified in Table III) to that of peak 3. The calculated ratios at $1.125\rho_c$ for the D_2 cases (*a*) and (*b*) in Table III, with multiplicities 2, 4, and 4 for the peaks 1, 2, and 4, respectively (to account for the experimental powder averaging procedure) are 0.056 and 0.050, while for the corrugation $1.4V_g(0)$ they are 0.076 and 0.068. The ratio for the neutron intensities at this density is in the range 0.07–0.10, so the model reproduces the primary data satisfactorily. For H_2/graphite at this density the calculated ratio is about 0.03 and the measured[4] ratio is in the range 0.05–0.70.

For reference, the elastic constants[27] for a triangular lattice, on a structureless substrate, with the same average density as this structure are given in Table IV for the SG model. The de Boer–Lennard-Jones model for D_2 has a negative bulk modulus at this density.

V. CONCLUDING REMARKS

These calculations of the energy and structure of monolayer lattices of deuterium and hydrogen, with a multiparameter potential model which reproduces a wide

TABLE III. Structure factor intensities[a] for uniaxial incommensurate lattice of density $1.125\rho_0$ cases.[b]

		H_2		D_2	
$S(k)$ peak[c]	Wave vector[d]	(*a*)	(*b*)	(*a*)	(*b*)
1	$\mathbf{t}_3-\mathbf{q}$	0.021	0.020	0.047	0.043
2	$\mathbf{t}_1-\mathbf{q}$	0.0064	0.0063	0.0099	0.0091
3	$\mathbf{t}_1$	0.514	0.530	0.596	0.611
4	$\mathbf{t}_3$	0.446	0.464	0.483	0.504
5	$\mathbf{t}_1+\mathbf{q}$	0.017	0.016	0.031	0.028
6	$\mathbf{t}_3+\mathbf{q}$	0.031	0.029	0.064	0.060
$R_{\rm SF}$[e]					
1		0.52	0.49	0.46	0.45
2		0.28	0.23	0.36	0.34
3		0.20	0.19	0.13	0.13
4		0.15	0.15	0.068	0.071
5		0.26	0.25	0.24	0.24
6		0.27	0.26	0.20	0.20

[a]Calculations with Eq. (3.20) for the minimum-energy structure, with trial function specified by Eqs. (3.22) and (3.15) and $V_g=-6.4$ K.

[b]Cases as in Table I.

[c]Enumeration of peaks as given in Refs. 1 and 2.

[d]Wave vectors of peaks, from Eqs. (3.17) and (3.19), with $\bar{m}=-\frac{1}{9}$.

[e]Debye-Waller factor ratio, Eq. (4.1).

TABLE IV. Elastic constants of a triangular monolayer lattice of density[a,b] $1.125\rho_c$.

	$H_2(a)$	$H_2(b)$	$D_2(a)$	$D_2(b)$
E[c]	−24.9	−9.5	−42.7	−28.1
ϕ[d]	1.01	4.39	−3.79	−0.54
B[e]	32.8	44.6	15.21	27.6
C_{33}	24.3	30.0	14.5	19.8
C_{11}	57.0	74.6	29.7	47.4
C_l^2/C_t^2[f]	2.41	2.74	1.83	2.36

[a]Density chosen to match the average density of the uniaxial incommensurate lattice, sketched in Fig. 1, for which results are reported in Table II.
[b]Interaction model and cases as in Table I.
[c]Energy per molecule in K.
[d]Spreading pressure in erg/cm^2; negative values for cases dilated related to the minimum energy lattices of Table I.
[e]Bulk modulus B, shear modulus C_{33}, and elastic constant C_{11} (all in erg/cm^2), calculated as described in Ref. 27.
[f]Calculated ratio of squares of the speed of longitudinal and transverse sound.

range of data for the three-dimensional bulk phases, give a fairly good account of available experimental data. The most uncertain input information is for the leading Fourier amplitude V_g of the lateral variation of the holding potential at the equilibrium overlayer height. As for other systems, a value based on atom-atom modeling of the holding potential seems to underestimate the lateral variations; the calculated Brillouin zone-center frequency gap is 10–25 % lower than experimental values. The two-dimensional lattice approximation may be suspect for the most closely spaced rows in the uniaxial incommensurate lattice we have treated.

We have extended the variational quantum mechanics for the ground state of a quantum solid to include effects of the modulation of the monolayer by the substrate. Further work might include the three-dimensional character of the layers and a more detailed account of the relaxation of rows at domain boundaries. However, the multiparameter variational searches, from our experience, would depend on very precise evaluations of small energy increments and other methods may then be more powerful. Qualitatively, the expectation that a highly compressible quantum monolayer solid has sharp domain walls is borne out in the present work.

ACKNOWLEDGMENTS

This work was supported in part by the National Science Foundation through Grant Nos. DMR-85-16116 and DMR-88-17761. The Monte Carlo calculations were performed at the San Diego Supercomputer Center. We thank Professor S. C. Fain, Jr. for several helpful comments.

APPENDIX A: THE ONE-DIMENSIONAL CHAIN

Consider the energy of the one-dimensional Frenkel-Kontorova chain[24,25] of N atoms:

$$E=J\sum_{n=1}^{N-1}(x_{n+1}-x_n-a)^2-A\sum_{n=1}^{N}\cos(2\pi x_n/b)\ . \quad \text{(A1)}$$

If the positions x_n are expressed in terms of scaled displacements u_n relative to the basic commensurate lattice by

$$x_n=nb+(bu_n)/(2\pi)\ , \quad \text{(A2)}$$

the energy is rewritten as

$$E=N[J(b-a)^2-A]+(Jb/\pi)(b-a)(u_N-u_1)+\Delta E\ , \quad \text{(A3)}$$

with

$$\Delta E/A=(l_F^2/2)\sum_{n=1}^{N-1}(u_{n+1}-u_n)^2+\sum_{n=1}^{N}(1-\cos u_n) \quad \text{(A4)}$$

and

$$l_F^2=(J/2A)(b/\pi)^2\ . \quad \text{(A5)}$$

The energy increment in the continuum approximation of slowly varying displacements along the infinite chain is

$$\Delta E_{\rm co}/A=\int_0^\infty dn\,[l_F^2/2(du/dn)^2+(1-\cos u)]\ . \quad \text{(A6)}$$

For the case of a single heavy wall with

$$u(\infty)-u(-\infty)=-2\pi\ , \quad \text{(A7)}$$

the continuum energy is minimized by a wall structure (here written as centered as $n=0$)

$$u(n)=4\tan^{-1}(\exp(-n/l_F))\ , \quad \text{(A8)}$$

with

$$\Delta E_{\rm co}=8Al_F\ . \quad \text{(A9)}$$

If the exact solution Eq. (A8) is approximated by a trial solution

$$u_t(n)=\pi[1-\tanh(n/l_t)]\ , \quad \text{(A10)}$$

the corresponding approximation to the continuum energy is minimized by

$$l_t=1.643l_F \quad \text{(A11)}$$

with a bound for the energy for

$$\Delta E_{\rm co}<8.008Al_F\ ; \quad \text{(A12)}$$

i.e., the upper bound is less than 1% larger than the exact solution. Alternatively, forcing the slope of the trial solution to match that of the exact solution at $n=0$ gives $l_t=(\pi/2)l_F$.

If the positions in the discrete lattice model, Eq. (A1), are varied to minimize the energy, the optimal positions satisfy

$$u_{n+1}-2u_n+u_{n-1}=1/l^2\sin u\ . \quad \text{(A13)}$$

For the discussion of Sec. IV we solve Eq. (A13) for a domain of six rows with a heavy wall centered between rows 3 and 4 and compare the resulting positions to those based on Eqs. (A10) and (A8). There are three domain structures to be compared: one based on Eq. (A10) with an optimized l_t, one based on Eq. (A8), and one based on

Eq. (A13) with $l = l_J$ adjusted to give the same smallest nearest-neighbor spacing as Eq. (A10).

APPENDIX B: MINIMIZATION OF THE VARIATIONAL ENERGY

The Monte Carlo calculation for each parameter set in the striped structure is performed on a periodically repeated cell of 144 particles, with an average over 450 000 configurations. The cases are ordered on a large grid according to the values of A, b, and l.

A least-squares fit[15] using a cubic polynomial in the variables A, b, and l is made over the grid for each expectation value, following Nosanow *et al.*[15] The resulting 20-term power series are used to interpolate the expectation values; the fitting procedure reduces effects of statistical randomness of the Monte Carlo averaging on the interpolations. The trial energy is formed by combining the fits to the individual expectation values and is given as another 20-term power series. The minimum trial energy is located with a three-dimensional Newton-Raphson search method on A, b, and l. The grids span the region of the final optimized parameters. For the H_2 case the grid has 436 points and for D_2 542 points; there is a small overlap of the grids. The grid for the parameter "b" extends $\pm 7\%$ from the central value, with a trial energy varying by 0.5% over this range. The grid for A extends $\pm 33\%$ from the central value and for l, $\pm 50\%$ from the central value. These are indications of the relative sensitivity of the trial energy to variations in the parameters; the uncertainties in the final values of the variational parameters reflect the relative sensitivities.

APPENDIX C: COMPUTATION OF THE BULK MODULUS

The bulk modulus of triangular lattices of H_2 or D_2 is constructed from finite difference approximations to the density derivative of the variational energy. For each set of A and b, the Monte Carlo averaging is performed over 450 000 configurations of a periodically repeated cell of 100 particles.

We use at least 50 A and b cases to identify the trial energy minimum at each density and fit the energy as a cubic polynomial over the density range. The Monte Carlo calculation is performed for a total of eight densities and more than 400 A and b cases.

[1] J. Cui and S. C. Fain, Jr., Phys. Rev. B **39**, 8628 (1989); J. Cui, Ph.D. thesis, University of Washington, 1988.

[2] J. Cui, S. C. Fain, Jr., H. Freimuth, H. Wiechert, H. P. Schildberg, and H. J. Lauter, Phys. Rev. Lett. **60**, 1848 (1988).

[3] H. P. Schildberg, H. J. Lauter, H. Freimuth, H. Wiechert, and R. Haensel, Jpn. J. Appl. Phys. **26**, Suppl. 3, 345 (1987).

[4] H. Freimuth, H. Wiechert, and H. J. Lauter, Surf. Sci. **189/190**, 548 (1987).

[5] H. J. Lauter, H. P. Schildberg, H. Godfrin, H. Wiechert, and R. Haensel, Can. J. Phys. **65**, 1435 (1987).

[6] M. Nielsen, J. P. McTague, and W. Ellenson, J. Phys. (Paris) Colloq. **38**, C4-10 (1977); M. Nielsen, J. P. McTague, and L. Passell, in *Phase Transitions in Surface Films*, edited by J. G. Dash and J. Ruvalds (Plenum, New York, 1980), p. 127.

[7] V. L. P. Frank, H. J. Lauter, and P. Leiderer, Phys. Rev. Lett. **61**, 436 (1988).

[8] H. Freimuth and H. Wiechert, Surf. Sci. **178**, 716 (1986).

[9] F. C. Motteler and J. G. Dash (unpublished and private communication); F. C. Motteler, Ph.D. thesis, University of Washington, 1986.

[10] X. Z. Ni and L. W. Bruch, Phys. Rev. B **33**, 4584 (1986).

[11] I. F. Silvera and V. V. Goldman, J. Chem. Phys. **69**, 4209 (1978), and references therein.

[12] Z.-C. Guo and L. W. Bruch, J. Chem. Phys. **77**, 1417 (1982).

[13] L. Mattera, F. Rosatelli, C. Salvo, F. Tommesini, U. Valbusa, and G. Vidali, Surf. Sci. **93**, 515 (1980).

[14] A. D. Novaco, Phys. Rev. Lett. **60**, 2058 (1988).

[15] L. H. Nosanow, L. J. Parish, and F. J. Pinski, Phys. Rev. B **11**, 191 (1975), and references therein.

[16] W. L. McMillan, Phys. Rev. **138**, A442 (1965).

[17] F. F. Abraham and J. Q. Broughton, Phys. Rev. Lett. **59**, 64 (1987).

[18] I. F. Silvera, Rev. Mod. Phys. **52**, 393 (1980).

[19] L. W. Bruch, Surf. Sci. **125**, 194 (1983), and references therein.

[20] M. Ross, F. H. Ree, and D. A. Young, J. Chem. Phys. **79**, 1487 (1983); D. A. Young and M. Ross, *ibid.* **74**, 6950 (1981).

[21] M. J. Norman, R. O. Watts, and U. Buck, J. Chem. Phys. **81**, 3500 (1984).

[22] T. Halpin-Healy and M. Kardar, Phys. Rev. B **34**, 318 (1986), and references therein.

[23] K. Kern, R. David, P. Zeppenfeld, and G. Comsa, Surf. Sci. **195**, 353 (1988).

[24] F. C. Frank and J. H. van der Merwe, Proc. R. Soc. London, Ser. A **198**, 205 (1949); **198**, 216 (1949).

[25] B. Joos, Solid State Commun. **42**, 709 (1982).

[26] L. W. Bruch, Phys. Rev. B **37**, 6658 (1988).

[27] L. W. Bruch and J. M. Gottlieb, Phys. Rev. B **37**, 4920 (1988).